Analysis of the ENSO Cycle in the NCEP Coupled Forecast Model

QIN ZHANG

RSIS/Climate Prediction Center, NCEP/NOAA, Camp Springs, Maryland

ARUN KUMAR, YAN XUE, AND WANQIU WANG

Climate Prediction Center, NCEP/NOAA, Camp Springs, Maryland

FEI-FEI JIN*

Meteorology Department, The Florida State University, Tallahassee, Florida

(Manuscript received 30 November 2005, in final form 29 August 2006)

ABSTRACT

Simulations from the National Centers for Environmental Prediction (NCEP) coupled model are analyzed to document and understand the behavior of the evolution of the El Niño–Southern Oscillation (ENSO) cycle. The analysis is of importance for two reasons: 1) the coupled model used in this study is also used operationally to provide model-based forecast guidance on a seasonal time scale, and therefore, an understanding of the ENSO mechanism in this particular coupled system could also lead to an understanding of possible biases in SST predictions; and 2) multiple theories for ENSO evolution have been proposed, and coupled model simulations are a useful test bed for understanding the relative importance of different ENSO mechanisms.

The analyses of coupled model simulations show that during the ENSO evolution the net surface heat flux acts as a damping mechanism for the mixed-layer temperature anomalies, and positive contribution from the advection terms to the ENSO evolution is dominated by the linear advective processes. The subsurface temperature–SST feedback, referred to as thermocline feedback in some theoretical literature, is found to be the primary positive feedback, whereas the advective feedback by anomalous zonal currents and the thermocline feedback are the primary sources responsible for the ENSO phase transition in the model simulation. The basic mechanisms for the model-simulated ENSO cycle are thus, to a large extent, consistent with those highlighted in the recharge oscillator. The atmospheric anticyclone (cyclone) over the western equatorial northern Pacific accompanied by a warm (cold) phase of the ENSO, as well as the oceanic Rossby waves outside of 15°S–15°N and the equatorial higher-order baroclinic modes, all appear to play minor roles in the model ENSO cycles.

1. Introduction

El Niño–Southern Oscillation (ENSO) is the dominant coupled air–sea interaction phenomenon in the tropical Pacific. Beginning from the hypothesis of Bjerknes (1969) that small perturbations in the tropical climate system may grow into either El Niño or La Niña via a positive feedback between ocean and atmosphere, different theories for understanding the initiation, evolution, and decay of the ENSO cycle have been proposed. Some of the proposed mechanisms for the ENSO cycle rely on the dominant role of ocean wave dynamics and include the delayed oscillator (Suarez and Schopf 1988; Hirst 1988; Battisti and Hirst 1989), discharge–recharge oscillator (Jin 1996, 1997a,b; Jin and An 1999), western Pacific oscillator (Wang and Weisberg 1994; Weisberg and Wang 1997), and advective–reflective oscillator (Picaut et al. 1996, 1997; also see Wang and Picaut 2004 for a review).

To what extent different mechanisms for understanding the ENSO cycle may be important from one ENSO event to another, or the possibility that one single mechanism may dominate in general, has been analyzed based on evolution of observed SSTs, surface currents, or heat content anomalies associated with differ-

* Current affiliation: Department of Meteorology, University of Hawaii at Manoa, Honolulu, Hawaii.

Corresponding author address: Qin Zhang, RSIS/Climate Prediction Center, NCEP/NOAA, 5200 Auth Road, Rm. 800, Camp Springs, MD 20746.
E-mail: qin.zhang@noaa.gov

DOI: 10.1175/JCLI4062.1

ent ENSO events. Several such studies using observational data have been reported (Wyrtki 1975; Hayes et al. 1991; Kessler and McPhaden 1995; Delcroix et al. 1994; Frankignoul et al. 1996; Wang and McPhaden 2000; Bonjean 2001; Hasegawa and Hanawa 2003) and have pointed to the complexity of the evolution of ENSO on interannual time scales.

Most of the observational studies related to the ENSO cycle ascribe an important role to upwelling and vertical mixing in the equatorial cold tongue. However, there is less agreement among observational results for regions away from the cold tongue region of the equatorial tropical Pacific. For example, McPhaden and Picaut (1990) suggested that zonal advection by anomalous currents is a dominant mechanism for interannual SST variation in the central and western equatorial Pacific. By analyzing buoy drifter and current meter records between January 1987 and December 1993, Frankignoul et al. (1996) also showed that large-scale advection by zonal currents contributes significantly to the development of SST anomalies in the central and eastern Pacific. On the other hand, Weisberg and Wang (1997) argued that zonal advection was not a significant cause of local changes in SST at 0°, 170°W for 1988–94. In a subsequent study Wang and McPhaden (2000) examined surface layer heat balance on interannual time scales in the equatorial Pacific associated with the warm and cold phases of ENSO using Tropical Atmosphere–Ocean (TAO) buoy array data. Their results highlight the potential complexity of the ENSO cycle in that all terms in the heat balance contributed to changes in SST anomalies.

Because of the paucity of spatial and temporal coverage of ocean observations, the analysis of the physical mechanism responsible for the ENSO cycle based on the observational data alone remains problematic. An alternative approach for analyzing the physical mechanism behind the ENSO cycle is to use coupled ocean–atmosphere model simulations. Using an intermediate coupled model, Battisti (1988) showed that the leading term in the SST tendency equation is the meridional advection over the central-eastern Pacific and the vertical advection at the far eastern Pacific. The leading role of meridional advection during the mature phase of ENSO was also shown by Lau et al. (1992) using ocean–atmosphere coupled general circulation model (CGCM) simulations. More recently, also from the analysis of CGCM simulations, Yu and Mechoso (2001) demonstrated that the buildup of subsurface temperature anomalies related to ENSO was dominated by vertical advection in the western Pacific and meridional advection in the central Pacific.

Although coupled model simulations provide a dynamically consistent representation for different phases of ENSO, a drawback of model-based analysis is that conclusions can be easily influenced by model biases and may not be representative of the ENSO mechanism in nature. To gain confidence in results obtained based on coupled model simulations, it is essential that the analysis be repeated with a wide range of coupled models. In the present paper, an analysis of the simulations with the coupled model currently operational at NCEP is made. A unique feature of this model is the small tropical climate drift (or bias) in model integrations spanning 30–40 yr (Wang et al. 2005). Furthermore, understanding of the ENSO mechanism in this particular coupled model is of importance as the coupled model is also used operationally to provide model-based guidance on the seasonal time scale (Saha et al. 2006). Better understanding of the ENSO mechanism in this particular coupled system could also lead to understanding of potential biases in SST predictions and may even provide guidance for the future development of the coupled forecast system. Analysis in this paper differs from Wang et al. (2005) in that our focus is on the analysis of diagnosis of processes responsible for the model-simulated ENSO cycle. Readers interested in a more detailed comparison of observed versus model-simulated ENSO characteristics are referred to Wang et al. (2005).

The remainder of the paper is organized as follows: the coupled model is briefly described in section 2. In section 3, the performance of the model is assessed in terms of its ENSO evolution. Section 4 describes the mixed layer heat budget analysis for the model-simulated ENSO cycle. Analysis of the physical mechanism responsible for the ENSO cycle is extended further based on the evolution of heat content anomalies in section 5. Discussion and conclusions are presented in section 6.

2. Data and model simulations

The coupled ocean–atmosphere model used in this study is the coupled Climate Forecast System model (CFS) developed at NCEP. The CFS is the current NCEP operational system that provides dynamical forecast guidance of oceanic and atmospheric anomalies on seasonal time scales. A description of CFS can be found in Wang et al. (2005) and Saha et al. (2006). Briefly, CFS consists of the NCEP atmospheric Global Forecast System model (GFS) as of February 2003, and version 3 of the Geophysical Fluid Dynamics Laboratory's Modular Ocean Model (MOM3; Pacanowski and Griffies 1998).

The atmospheric component GFS uses a triangular

horizontal spectral truncation of 62 waves (T62) and has 64 vertical levels with enhanced resolution near the lower and the upper boundaries of the vertical domain. The top-most boundary of the model extends to 0.2 hPa. The model also includes a comprehensive package of parameterization schemes related to different atmospheric processes.

The MOM3 ocean model is configured as a global ocean model with north–south domain extending from 74°S to 64°N. The model has 40 layers in the vertical with 10-m resolution in the upper 240 m. Latitudinal spacing is 1/3° between 10°S and 10°N, gradually increasing through the Tropics until becoming fixed 1° poleward of 30°S and 30°N. The longitudinal spacing is 1°. Vertical mixing follows the nonlocal K-profile parameterization of Large et al. (1994). The horizontal mixing of tracers uses the isoneutral method pioneered by Gent and McWilliams (1990; see also Griffies et al. 1998). The horizontal mixing of momentum uses the nonlinear scheme of Smagorinsky (1963).

The atmospheric and oceanic components are coupled without any flux adjustment. The two components exchange daily averaged quantities once per day. Because of the difference in latitudinal domain, full interaction between atmospheric and oceanic components is confined to 65°S to 50°N. Poleward of 74°S and 64°N, SSTs for the atmospheric component are taken from observed climatology. Between 74° and 65°S, and 64° and 50°N, SSTs for the atmospheric component are the weighted average of the observed SST climatology and the SST from the ocean component of CFS, with weights linearly varying in latitude such that SSTs at 74°S and 64°N equal the observed climatology, and at 65°S to 50°N equal SSTs from the ocean model. Sea ice extent is prescribed from the observed climatology.

In the present study a set of three 30-yr coupled simulations is analyzed. These simulations started from initial conditions of 1 January of 1988, 1995, and 2002. The oceanic initial states were taken from the NCEP Global Ocean and Data Assimilation System (GODAS) and the atmospheric initial conditions from the NCEP/Department of Energy (DOE) Reanalysis-2 (Kanamitsu et al. 2002). Each of the three coupled model integrations is for a 40-yr period, and the first 10 yr of the model integration are not included in the analysis. This allows analysis of data after the coupled model simulations have entered their state of climatological interannual variability. Although the model drift for the first 40 yr of integrations is small, to avoid complications due to larger potential drift that may exist in longer integrations, we restrict each coupled integration to a 40-yr period. Our analysis is based on monthly mean fields and all anomalies are computed with respect to each model's own climatology.

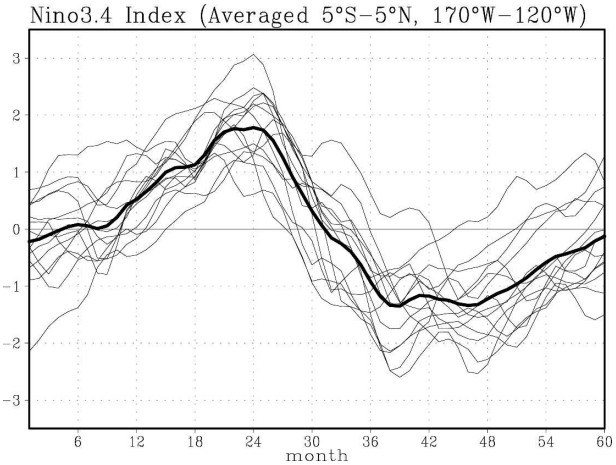

FIG. 1. Evolution of the Niño-3.4 SST index of the 14 warm and cold events (thin lines,) and their composite (thick black line) for 60-month (5 yr) life span associated with the model-simulated ENSO cycle (K).

3. Coupled model simulation of the ENSO variability

Prior to presenting the heat budget analysis, the ENSO cycle in the coupled model simulation is described. The analysis complements the analysis of Wang et al. (2005), who for the same coupled model simulations, also discussed some basic features of model biases and simulation of the ENSO variability.

For the three coupled simulations we first identify the ENSO events. Model ENSO events are identified based on the time series of the model-simulated Niño-3.4 SST index. Specifically, whenever a warm, as well as the subsequent cold, peak in the Niño-3.4 time series exceeds one standard deviation, a warm event followed by a cold event (referred to as the ENSO cycle) is identified. If a warm or cold event occurs in isolation, such isolated events are not included in our analysis, a scenario that occurs quite infrequently. Based on this criterion, a total of 14 warm–cold ENSO cycle events are identified.

Shown in Fig. 1 are the time traces of the Niño-3.4 SST index for all 14 events (in thin lines). Also shown is their composite (in thick line). The x axis in Fig. 1 spans a 60-month period. The events are aligned such that month 25 corresponds to January near the peak of the warm phase. For the composite ENSO cycle simulated by the model, a warm event starts to build in the fall of year 1 ($\sim$ month 9) and is approximately 6 months earlier than that in the observations, where

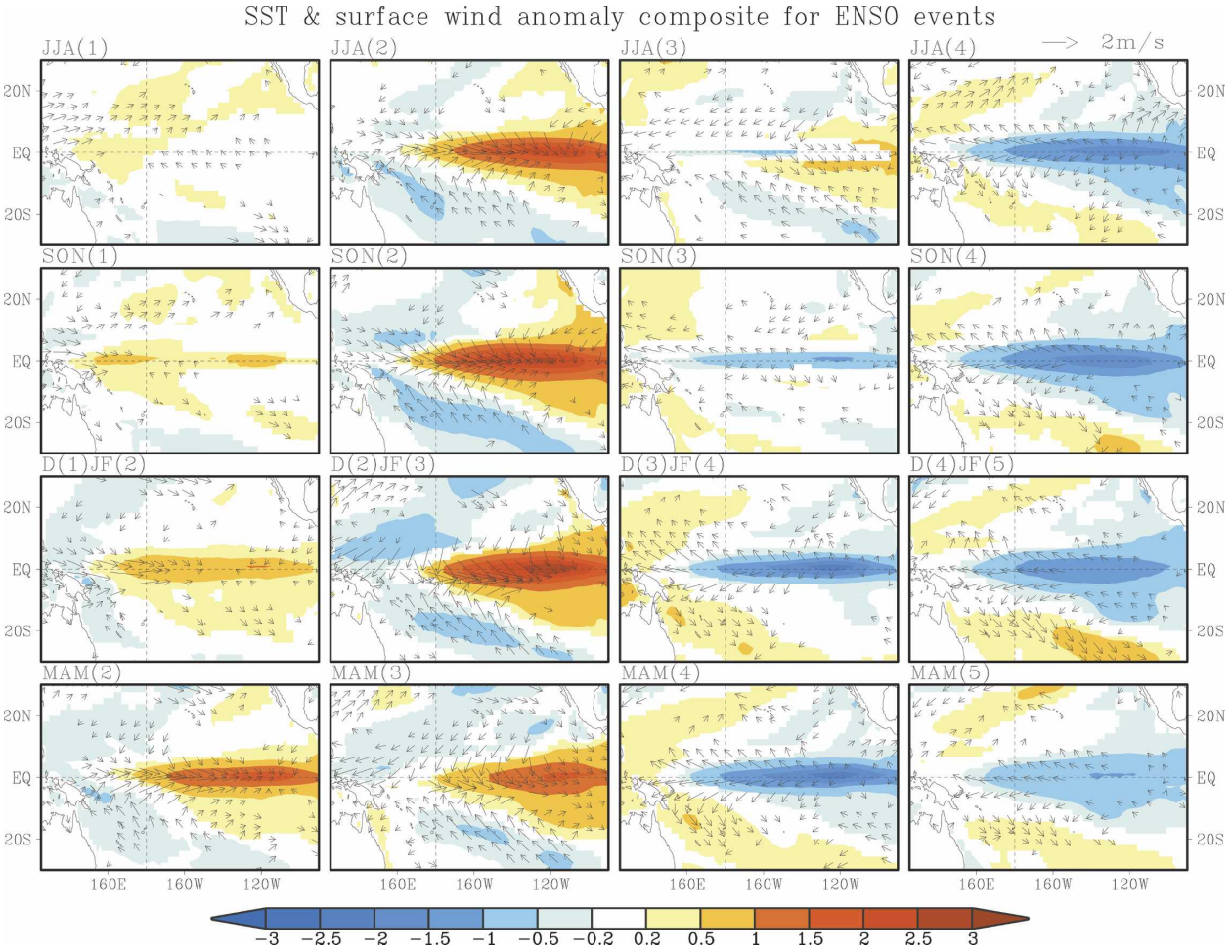

FIG. 2. Composite of seasonal averaged SST (shading, K) and surface wind (arrows, m s^{-1}) anomalies associated with the model-simulated ENSO cycle. The three letters indicate the season, and the numeral in parentheses indicates the year in the 5-yr ENSO cycle. Only the values that are statistically significant at the 95% confidence level for a Student's *t* test are shown.

warm events start to develop around March of year 2 (month 15; Rasmusson and Carpenter 1982). The warm Niño-3.4 SST anomalies reach their peak during the northern winter of years 2/3, following which the Niño-3.4 anomaly evolves to a cold phase. The duration of the peak in the cold Niño-3.4 SST anomalies is broader compared to the warm events, and furthermore, similar to the observations, it is weaker in amplitude than for the warm event.

The spatial pattern of the tropical Pacific seasonal mean SST anomalies for the composite ENSO cycle is shown in Fig. 2. Also shown are the composite surface wind anomalies. The three letters on the top of each panel indicate the seasonal mean over which anomalies are computed, and numerals 1 to 5 in parentheses denote the year in the composite ENSO cycle. For example, SON(1) refers to a seasonal mean for September–November (hereafter, 3-month periods are denoted by the first letter of each respective month) and for year 1 in the 5-yr ENSO cycle. For both SSTs and surface wind, only anomalies that are above 95% statistical significance are shown.

For convenience of discussion, the entire 5-yr ENSO cycle is divided into five different phases: (a) a development phase for the warm event extending from JJA(1) to SON(2); (b) the warm event mature phase for D(2)JF(3); (c) a transition from a warm event to a cold event from MAM(3) to SON(3); (d) the cold event mature phase from D(3)JF(4) to MAM(4); and (e) a decay phase for the cold event from JJA(4) to MAM(5).

During the development phase of the warm event, warm SST anomalies start to build up around the date line in D(1)JF(2). Westerly (easterly) surface wind anomalies also accompany the warm SSTs near the date line (eastern equatorial Pacific). In the spring and fall of

year 2, weak SST anomalies amplify and spread throughout the equatorial tropical Pacific. Strengthening of warm SSTs is also associated with the strengthening of westerly wind anomalies throughout the Pacific basin with the exception of anomalous easterlies confined near the west coast of South America. In phase with the warming of the equatorial SSTs, well-defined cold SST anomalies in the form of a horseshoe pattern, straddling the warm SSTs, also begin to establish. Warm SST anomalies peak around December of year 2. A particular feature to note is that the warmest anomalies are located around 150°W, and not close to the South American coast. At the peak of the warm event around D(2)JF(3), easterly surface wind anomalies also appear over the warm pool, and consistent with the observations, are associated with the establishment of an anticyclone over the Philippine Sea (Wang et al. 2000; Wang and Zhang 2002).

Following the peak phase of the warm event in the winter of years 2/3, SST anomalies start to decrease and transition to the cold phase of the ENSO cycle. By SON(3) the westerly surface wind anomalies are replaced by the easterly anomalies throughout the equatorial tropical Pacific. For the ENSO cycle simulated by the coupled model, the mature phase of cold event lasts almost through year 4, and has a broader peak than that corresponding for the warm event. The cold SST anomalies in the eastern Pacific and warm SST anomalies in the western Pacific, as well as the anomalies off the equatorial latitudes, are almost opposite to the SST conditions during the warm phase of the ENSO cycle. Finally, in year 4 of the ENSO cycle, the cold SST anomalies gradually start to decrease and reach neutral conditions by the end of year 5 (Fig. 1).

Corresponding to the evolution of SSTs following the ENSO cycle, the evolution of subsurface heat content (averaged temperature from bottom of mixed layer to 300 m, in kelvins) and equatorial subsurface temperature anomalies is shown in Figs. 3a and 3b, respectively. Prior to the occurrence of the warm SST anomalies during the development phase of the ENSO, positive subsurface temperature anomalies throughout most of the equatorial Pacific, and particularly in the western Pacific, are already established, for example, JJA(1) and SON(1) in Figs. 3a and 3b. As the development phase of the ENSO cycle proceeds, the subsurface temperature anomalies amplify and expand eastward to reach the coast of South America around D(2)JF(3), and ENSO reaches its mature phase of warm event as also depicted by the SSTs (Fig. 2). The east–west contrast in the equatorial ocean heat content, and associated sea level, yields a strong zonal pressure gradient that is in a quasi balance with the strong westerly wind stress anomaly following the so-called the equatorial Sverdrup balance (Philander 1990).

Starting with D(1)JF(2), a cold subsurface temperature anomaly, or negative heat content anomaly, also starts to develop in the western Pacific as the result of wind stress forcing associated with the onset of the warming. This initial indication of discharge of warm pool heat content intensifies as the ENSO warm phase matures and continues until the cold phase becomes well developed by D(3)JF(4). There is also a clear indication of an anticyclone over the Philippine Sea associated with the ENSO mature phase. This anticyclone may force some equatorial upwelling waves when associated with significant easterly winds in MAM(3), as suggested by Wang and Weisberg (1994), and by Weisberg and Wang (1997), who speculated that this anticyclone is critical for the ENSO phase transition. However, the anticyclone also clearly forces the off-equatorial downwelling Rossby waves, as indicated from the positive heat content anomalies at about 10°N at the western end of the warm pool in MAM(3) and JJA(3). Solomon and Jin (2005) suggested that the latter may slow the discharge process and thus prolong the ENSO cycle. It appears that the opposite effects of the Philippine Sea anticyclone suggested in the two studies may largely compensate, and thus, play a relatively insignificant role in the evolution of the ENSO cycle in the model simulations.

Following the peak phase of the warm event in D(2)JF(3), the warm subsurface anomalies in the eastern Pacific decay, and by JJA(3), are replaced by the cold subsurface anomalies. The aftermath of the warm event, the discharge of the equatorial heat content, generates a heat content deficit across the entire equatorial Pacific, which is clearly evident in Fig. 3b. The subsurface cold-water anomalies left after the El Niño phase are brought up to the surface leading to the initiation of the La Niña phase by SON(3). As will be further discussed in section 4, this phenomenological description of the ENSO cycle is consistent with that of the conceptual recharge oscillator (e.g., Jin 1997a,b).

The analysis of the model-simulated ENSO cycle in Figs. 1–3 indicates that the model simulations have a well-defined ENSO cycle, and certain characteristics of the simulated ENSO cycle also match their observational counterparts. For example, the amplitude of the Niño-3.4 SST anomalies is approximately 1.5°C, and the warm and cold events are phase locked with the annual cycle. In the next section, based on heat budget analysis for the mixed layer, we attempt to understand which terms in the temperature tendency equation are important in the evolution of the model-simulated ENSO cycle.

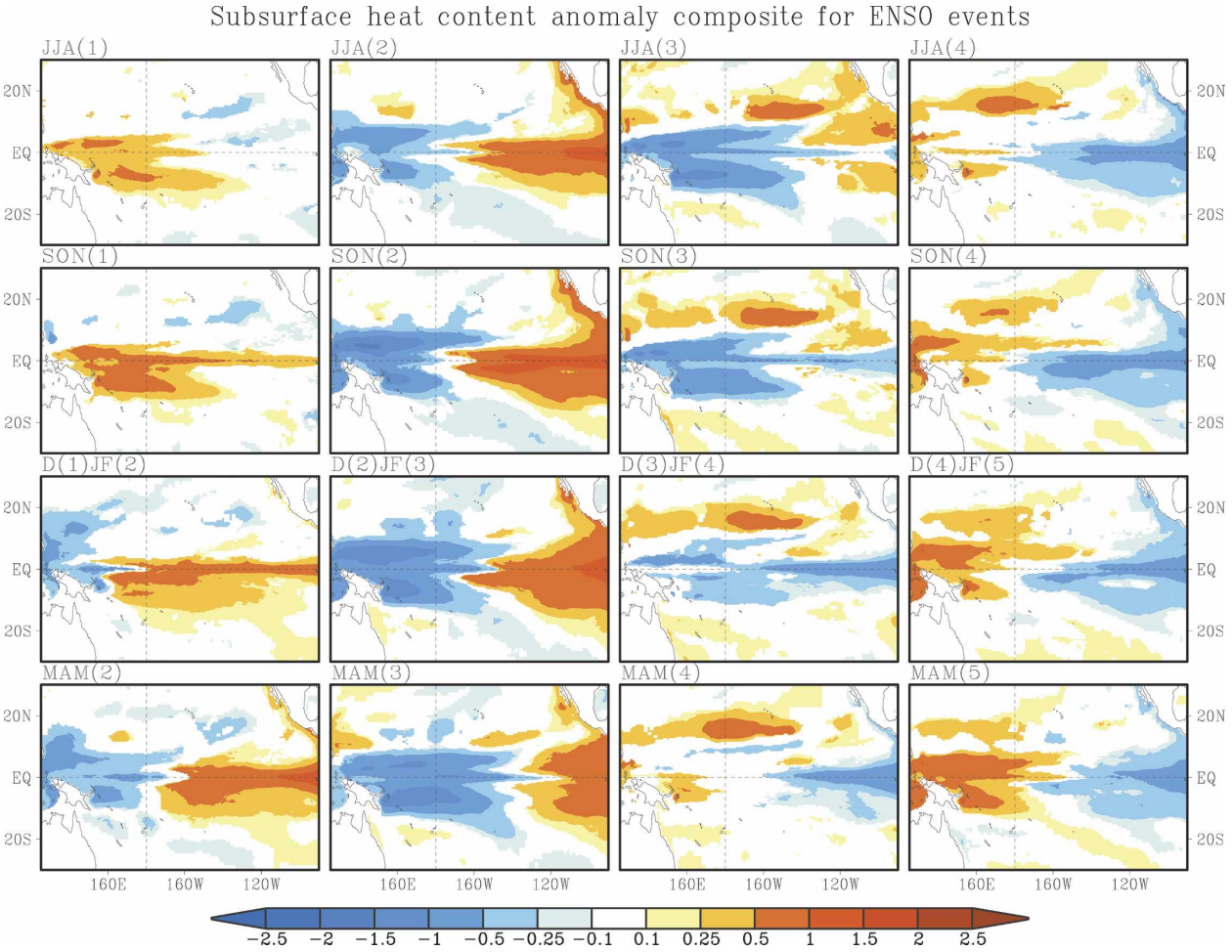

FIG. 3. (a) Composite of seasonal averaged subsurface heat content (averaged temperature from bottom of mixed layer to 300 m; shading, K) anomalies associated with the model-simulated ENSO cycle as in Fig. 2. (b) Same as in Fig. 2, but for the ocean temperature anomaly along the equator (K).

4. Mixed-layer heat budget associated with ENSO

The heat budget of the mixed layer is analyzed next in order to understand the physical processes responsible for the ENSO cycle in the coupled model simulations. The time tendency of the ocean temperature of the mixed layer is determined by horizontal advections, vertical mixing across the mixed layer, and the net surface heat fluxes. We first define a mixed-layer depth H where the ocean temperature is 0.5°C less than the surface temperature. With this definition, the annual mean of the model simulated mixed-layer depth is shown in Fig. 4. Also shown is the annual mean of ocean currents vertically averaged over the mixed-layer depth.

On an annual mean basis, the shallower mixed layer of about 15 m is confined to the easternmost part of the equatorial tropical Pacific. This shallow mixed layer deepens westward to about 50 m. A deeper mixed-layer depth of 70–80 m is located approximately 5° off the equator in the central Pacific. The basic features of the mixed-layer depth agree well with the observational analysis of Levitus and Boyer (1994). Because of time-varying horizontal mass convergence, the mixed-layer depth also undergoes significant seasonal variations (not shown).

The simulated annual ocean currents, vertically averaged over the mixed-layer depth, and displayed by arrows in Fig. 4, can be attributed to the ocean response to the surface wind forcing. Two branches of westward ocean currents, the South Equatorial Current (SEC) and the North Equatorial Current (NEC), located at 8°S and 4°N, respectively, are well simulated and are maintained by the off-equatorial divergence caused by Ekman transport. The Northern Equatorial Counter Current (NECC) between 5° and 10°N is also well simulated (Bonjean and Lagerloef 2002).

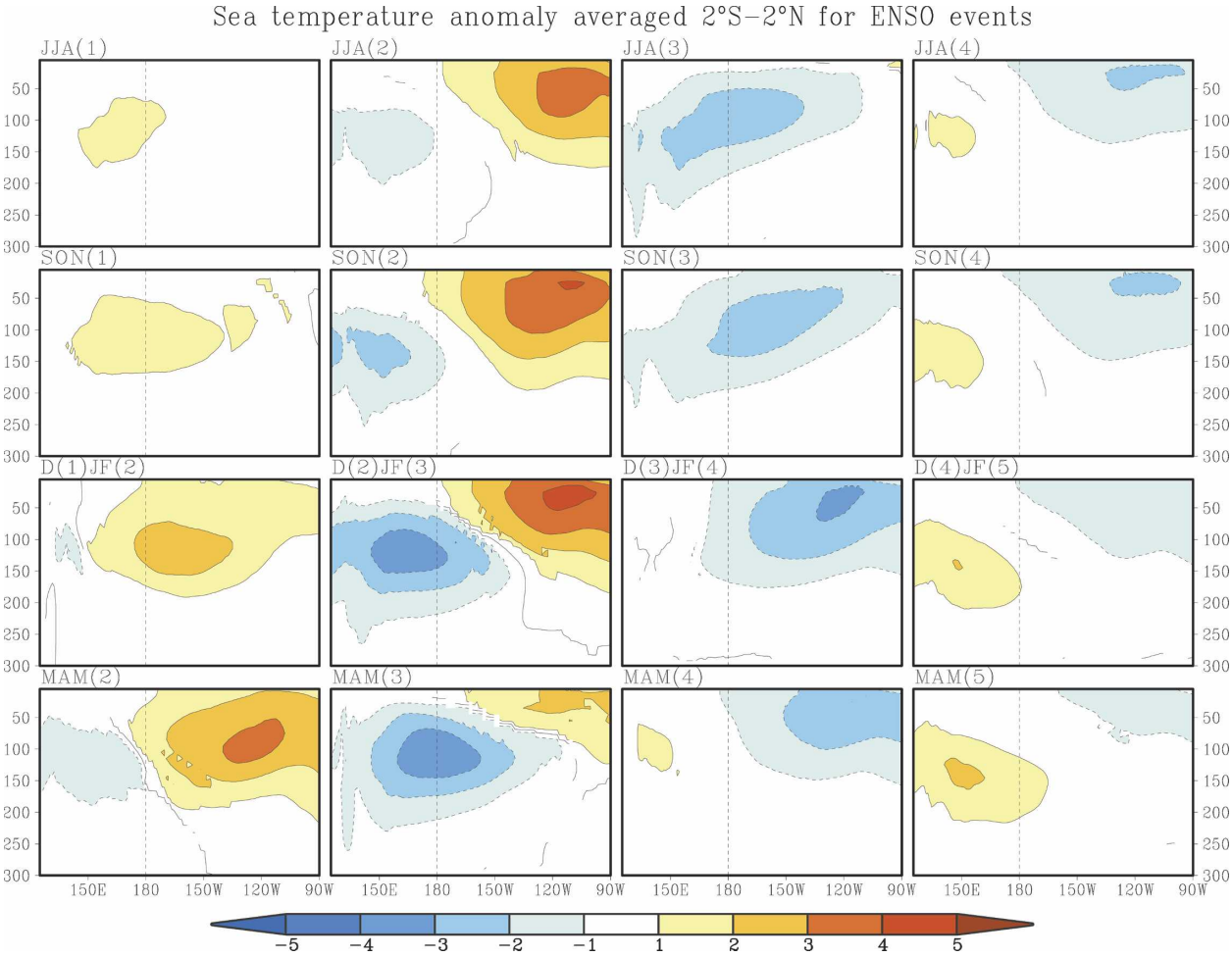

FIG. 3. (*Continued*)

The heat budget for the mixed layer is analyzed next. The vertical integral of the temperature tendency equation from the ocean surface to the bottom of the mixed layer at $z = -H$ is given by (Vialard et al. 2001)

$$\frac{\partial T}{\partial t} = -U\frac{\partial T}{\partial x} - V\frac{\partial T}{\partial y} + \frac{Q}{\rho C_p H} - \left(\frac{T - T_h}{H}\frac{dH}{dt} + W_h\frac{\partial T_h}{\partial z} + \frac{k}{H}\frac{\partial T_h}{\partial z}\right), \quad (1)$$

where T_h is the temperature immediately below the mixed layer, W_h is the vertical velocity at the base of the mixed layer, U is the zonal current, V is the meridional current, and T is the temperature in the mixed layer. Furthermore, k is the vertical diffusion coefficient and is computed following the KPP scheme (Large et al. 1994), and ρ_o and C_P are the density and heat capacity of the seawater. The net surface heat flux is denoted by Q and is the sum of shortwave and longwave radiation and sensible and latent heat flux.

Starting from (1), an equation for the time tendency of the monthly mean temperature anomaly T' can be derived, and is given by

$$\frac{\partial T'}{\partial t} = Q'_{\text{zon}} + Q'_{\text{mer}} + Q'_{\text{ver}} + Q' + R', \quad (2)$$

where T' is monthly mean anomaly for the mixed-layer temperature and is computed relative to the climatological monthly mean. The first two terms on the right-hand side correspond to zonal and meridional anomalous advections. The third term is related to the time tendency due to anomalous vertical advection. Each advection term is comprised of several component terms that, individually, will be discussed later. The fourth term on the right-hand side of (2) is the monthly mean net surface heat flux anomaly, while the last term R' is the residual term that cannot be resolved by monthly mean fields and is the monthly mean anomaly of submonthly transients, for example, tropical instability waves.

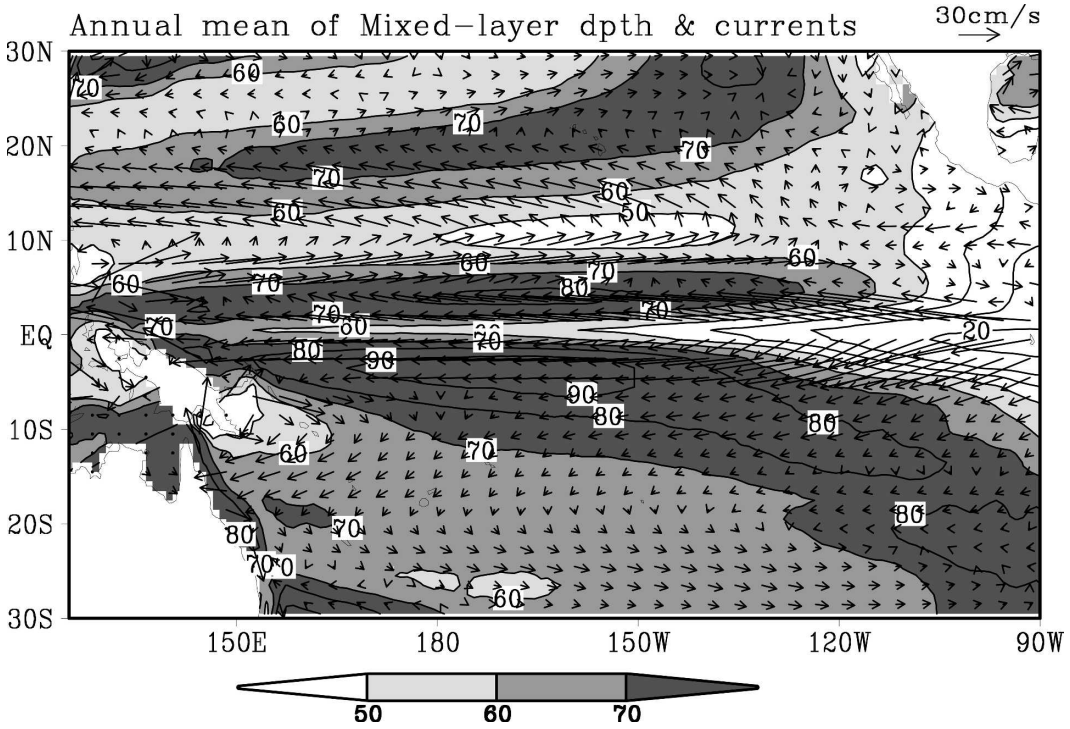

FIG. 4. Annual mean of mixed-layer depth (shading, m) and ocean currents (arrows, cm s^{-1}) for a 30-yr free run integration of CFS.

Starting from the monthly mean data from the coupled model simulations, all terms in (1), with the exception R', can be computed on a month-by-month basis. For one of the coupled model simulations, the time series of the mixed-layer temperature anomaly (or the SSTs) together with the integration of the first four tendency terms on the right-hand side of (2), averaged over the Niño-3.4 region, are shown in Fig. 5. There is good correspondence between the two, and the temporal correlation between them is 0.91. This implies that the impact of the residual term is small, and relative to the influence of other terms on the right-hand side of (2), can be ignored.

a. Heat budget for the composite ENSO cycle over the Niño-3.4 region

To compute the heat budget associated with the composite ENSO cycle, we first compute each term (except R') on a month-by-month basis. This computation is based on the monthly mean archives from the three coupled simulations, and for each simulation 30 yr of data are used. For the composite ENSO cycle, temperature tendency and different forcing terms are averaged over the 14 ENSO events shown in Fig. 1.

The mixed-layer temperature tendency and forcing terms for the composite ENSO cycle area averaged

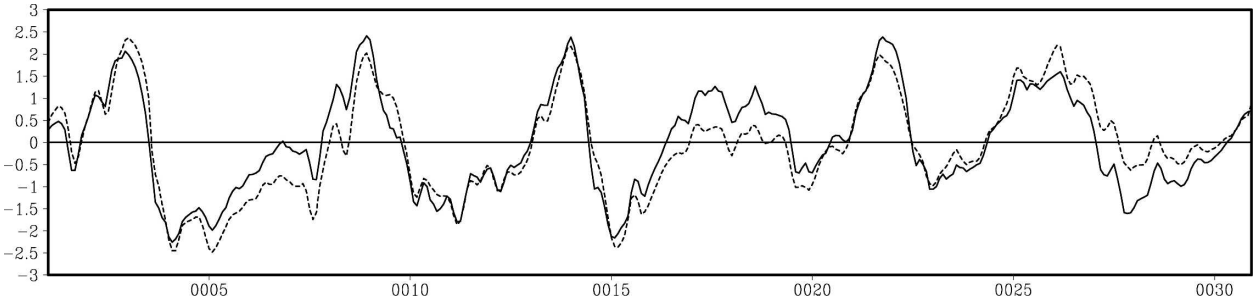

FIG. 5. The mixed-layer temperature anomaly (solid line) and the integration of the right side (dashed line) of (2) averaged over the Niño-3.4 region (K). The correlation coefficient between two time series is 0.91.

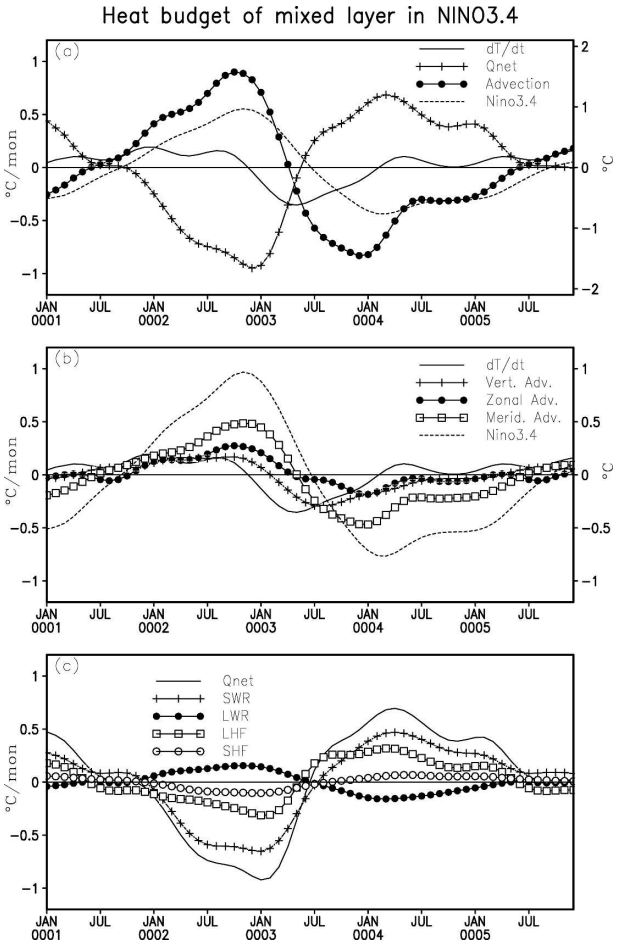

FIG. 6. (a) Temporal evolution of heat budget of the mixed layer averaged over the Niño-3.4 region. The solid and the dashed lines are the SST–tendency and Niño-3.4 SST index, respectively. The other two lines with symbols are the net heat flux and oceanic heat advection contribution to mixed-layer tendency, respectively. (b) Contribution of advection terms to the mixed-layer temperature in the Niño-3.4 region. The solid and dash lines are the same as in (a), and the other three curves with symbols are the vertical, zonal, and meridional heat advections, respectively. (c) Lines with symbols are shortwave radiation, longwave radiation, latent heat flux, and sensible heat flux components of the net heat flux tendency (solid line).

over the Niño-3.4 regions are shown in Fig. 6. The mixed-layer temperature tendency for the Niño-3.4 has a much broader peak during the development phase of the warm event than during the development phase of the cold event. On the other hand, temperature tendency is much larger during the decay phase of the warm event than during the decay phase of the cold event. This is consistent with the evolution of the Niño-3.4 SSTs in Fig. 1, where warm events tend to start much earlier, while the peak of cold events tends to linger and decay slowly toward a neutral condition.

The mixed-layer temperature tendency is essentially a sum of two large but opposite terms: net anomalous advection [defined as the sum of the first three terms on the right-hand side of (2)] that contributes to an increase in the temperature of the mixed layer, and net anomalous heat flux that tends to reduce the temperature (Fig. 6a).

The three advection terms and individual components of the heat flux are shown in Figs. 6b and 6c, respectively. In general, all three advection terms tend to be in phase with the mixed-layer temperature anomaly with the largest contribution coming from the anomalous meridional advection. For example, during the development phase of the warm event, anomalous meridional advection implies a positive temperature tendency, and is due to the decrease in poleward transport of the warmer equatorial anomalous temperatures by mean meridional currents. The dominance of meridional advection agrees with the earlier studies associated with the ENSO heat budget (Kang and An 2001; Wang and McPhaden 2000; An and Jin 2001).

Out of the three advection terms, the anomalous vertical advection is the least dominant term, and as will be discussed later, is because of the meridional average over a broad equatorial region extending from 5°S to 5°N that corresponds to the Niño-3.4 region. On the other hand, if the meridional domain of averaging is reduced to a narrower region, the importance of vertical advection across the mixed-layer interface becomes apparent, that is, considering the Niño-3.4 region as a whole, anomalous vertical advection in a narrow equatorial belt becomes an implicit source for the dominance of the anomalous meridional advection.

The anomalous net heat flux represents a negative feedback for the mixed-layer temperature anomalies. The four separate components of heat flux are shown in Fig. 6c. Except for the longwave radiative flux, the other three components of net heat flux contribute to the negative feedback. The anomalous shortwave radiative heat flux is the largest negative feedback and is related to the shift in tropical convection over to warmer SSTs that are associated with warm events. This shift in convection leads to a cutoff of downward solar radiation because of increased cloudiness. Increased cloudiness also leads to trapping of longwave radiative flux leading to its increase during the warm events. The reverse tends to happen for the cold events. Area-averaged over the Niño-3.4 region, the latent heat flux also represents a negative feedback while negative contribution from the sensible heat flux tends to be small. Explanation of the negative feedback related to the anomalous latent heat flux is not straightforward. On one hand, warm SSTs induce weaker surface wind

speed as a result of the associated westerly anomalies on top of the mean easterly wind, causing less evaporation and thus positive latent heat flux anomalies into the ocean. On the other hand, warmer SSTs increase evaporation for a given amplitude of wind speed, leading to negative latent heat flux anomalies into the ocean. The net negative latent heat flux anomalies during the development phase of the warm event in Fig. 6c indicate that the change in latent heat flux due to SST anomalies dominates over the change due to the surface wind speed anomalies.

The analysis of the heat budget so far relates to the mixed-layer temperature anomalies averaged over the Niño-3.4 region. In the subsequent analysis, we describe the spatial distribution of different forcing terms in (2). Particularly, we focus on the anomalous advections and also analyze their subcomponents. Since the net heat flux tends to be a negative feedback to the mixed-layer temperature anomalies throughout the ENSO cycle, and also throughout the tropical Pacific, for the sake of brevity, results for net heat flux are not shown.

b. *Spatial structure of anomalous advections for the composite ENSO cycle*

The time evolution of mixed-layer tendency and forcing terms averaged over the Niño-3.4 region is a succinct way to illustrate the temporal evolution of heat budget anomalies. To illustrate the spatial evolution of anomalous advections, a convenient alternative is to extract the mode of variability in the mixed-layer temperature tendency that is related to the ENSO cycle, and then to analyze the corresponding spatial patterns for different tendency terms. This approach is followed to illustrate the spatial variability of anomalous advections.

Empirical orthogonal function (EOF) analysis is used to identify the mode of mixed-layer temperature tendency that relates to the ENSO cycle. For three coupled simulations, EOF analysis for monthly mean fields is done over the tropical Pacific region extending from 30°S to 30°N and 120°E to 90°W. The dominant EOF mode for the mixed-layer temperature tendency is shown in Fig. 7a and explains 13%–15% of domain-averaged variance in the three simulations (although the local explained variance of the mixed-layer temperature variability over the Niño-3.4 region exceeds 90%). The spatial pattern of the first EOF has the largest loading in the equatorial eastern Pacific and exhibits characteristics of the spatial pattern of ENSO SSTs (see Fig. 2) with colder mixed-layer temperature tendencies straddling the warmer tendencies in the equatorial Pacific.

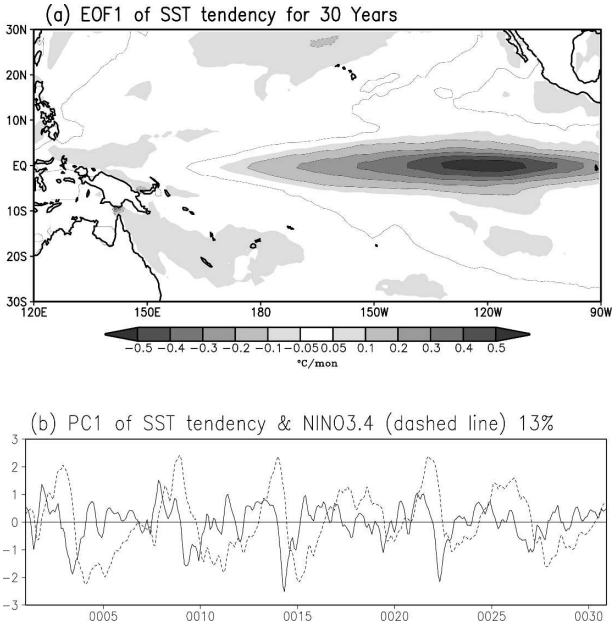

FIG. 7. (a) The first EOF of the mixed-layer temperature tendency in the tropical Pacific (30°S–30°N, 120°E–90°W). (b) Time series of the first EOF (solid line) and Niño-3.4 SST index (dash line). The first EOF of the mixed-layer temperature tendency accounts for 13% over the spatial domain and in excess of 90% variance over the Niño-3.4 region.

To illustrate further that the first EOF is indeed related to the mixed-layer temperature tendency of the ENSO cycle, its time series together with the time series of Niño-3.4 SSTs is shown in Fig. 7b for one of the coupled model simulations. As expected, time tendency for the mixed-layer temperature leads the Niño-3.4 SST anomalies. Temporal correlation between the two time series maximizes when the mixed-layer temperature tendency leads the Niño-3.4 SSTs by 6 months and is 0.65.

The anomalous advection terms associated with the ENSO cycle are next obtained as regressions against the time series corresponding to the first EOF. Anomalous advection terms are also separated into their components to gain better understanding. For example, the zonal advection term in (2) can be written as

$$Q'_{\text{zon}} = -U_m \frac{\partial T'}{\partial x} - U' \frac{\partial T_m}{\partial x} - \left[U' \frac{\partial T'}{\partial x} - \left(U' \frac{\partial T'}{\partial x} \right)_m \right], \tag{3}$$

where variables with a subscript m refer to the climatology of monthly means, and the variables with a prime denote the monthly mean anomaly. The first term on the right-hand side of (3) is the tendency due to the advection of the monthly mean mixed-layer tem-

perature anomaly by the climatological zonal current. The second term on the right-hand side of (3) represents the tendency due to the advection of climatological mixed-layer temperature by the anomalous monthly mean zonal current. Finally, the last term in (3) is the anomalous nonlinear advection of the monthly mean mixed-layer temperature anomaly by the anomalous monthly mean zonal currents.

Similar to the decomposition of the zonal advection term in (3), the meridional and vertical advection terms can also be written as

$$Q'_{\text{mer}} = -V_m \frac{\partial T'}{\partial y} - V' \frac{\partial T_m}{\partial y} - \left[V' \frac{\partial T'}{\partial y} - \left(V' \frac{\partial T'}{\partial y} \right)_m \right] \tag{4}$$

$$Q'_{\text{ver}} = -W_m \frac{\partial T'_h}{\partial z} - W' \frac{\partial T_{\text{hm}}}{\partial z} - \left[W' \frac{\partial T'_h}{\partial z} - \left(W' \frac{\partial T'_h}{\partial z} \right)_m \right] - \frac{0.5}{H} \frac{\partial H'}{\partial t}. \tag{5}$$

In (5), T'_h is the temperature anomaly just below the mixed layer, while T_{hm} is its climatological value.

For different terms on the right-hand side of (3)–(5), regression patterns with the time series of the first EOF of mixed-layer temperature tendency are shown in Figs. 8–10. All the plots can be interpreted as the contributions from different terms during the developing warm phase of the ENSO cycle. Of the three components of the zonal advection term, the advection of the climatological mixed-layer temperature due to the anomalous monthly mean zonal current dominates (Fig. 8, middle) in the equatorial tropical Pacific east of the date line. The contribution of the other two terms in (3) is generally less important (Fig. 8, top and bottom).

The most important contribution for the meridional advection is due to the advection of anomalous mixed-layer temperature by the climatological meridional currents (Fig. 9, top), with contributions from the other two terms playing a less important role. The contribution from the first term has the largest amplitude just north and south of the equator. Furthermore, for the warm phase of the ENSO cycle, the contribution for a positive tendency is because of the increased anomalous temperature gradient near the equator. The reverse happens for the cold events.

The regression plots for the vertical advections are shown in Fig. 10. As the contribution from the change in the mixed-layer depth is an order of magnitude smaller [i.e., the last term in the right-hand side of (5)], the spatial map corresponding to this term is not shown. In a narrow region confined to the equator, the mean vertical advection acting on the temperature anomaly

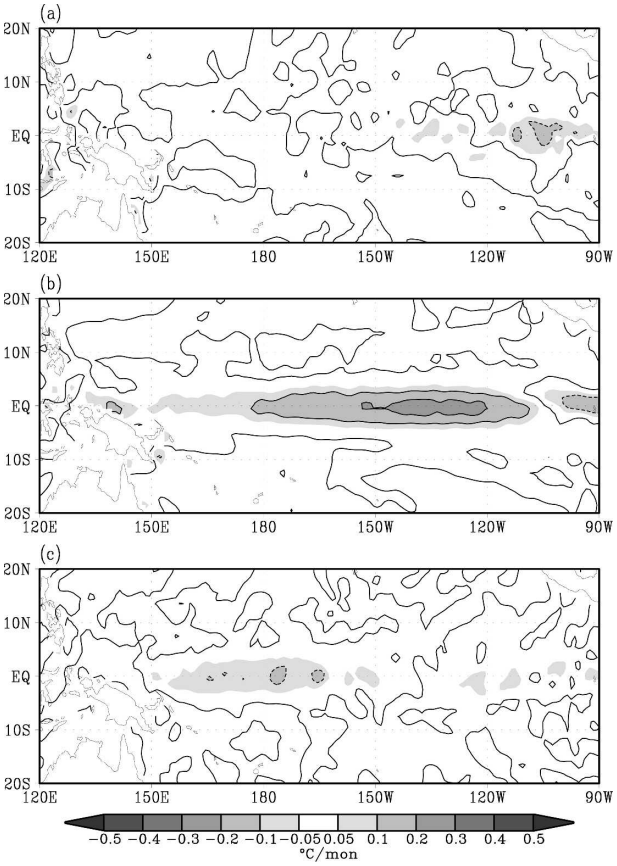

FIG. 8. Spatial pattern of the regression between different components of the zonal heat advection (a) $-U_m \partial T'/\partial x$, (b) $-U' \partial T_m/\partial x$, and (c) $-[U' \partial T'/\partial x - (U' \partial T'/\partial x)_m]$ with the time series of the first EOF of the mixed-layer temperature tendency.

across the mixed layer dominates and contributes to positive mixed-layer temperature tendency (Fig. 10, top). The mean vertical velocity in this region is always upward, and consequently, the warmer subsurface temperature anomaly is brought to the surface. In contrast to the vertical advection of the anomalous subsurface temperature by the mean vertical velocity, the vertical advection due to the anomalous vertical advection dominates in the eastern Pacific (Fig. 10, middle). Finally, the contribution from the nonlinear term is the smallest.

To summarize, an analysis of the mixed-layer temperature tendency points to the dominance of linear advective terms in the equatorial basin. All the advective terms are in phase with the temperature tendency. On the other hand, net heat flux forcing acts opposite to the temperature tendency and is a negative contribution to evolving mixed-layer temperature anomalies. To provide a complete picture of how the different advective processes affect the ENSO cycle in the coupled

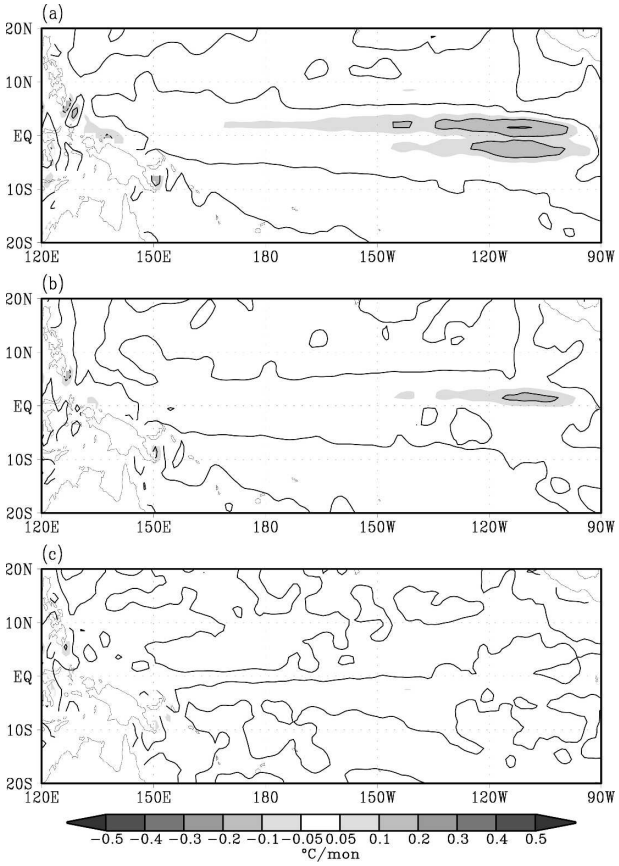

FIG. 9. Same as in Fig. 8, but for different components of the meridional heat advection: (a) $-V_m\partial T'/\partial y$, (b) $-V'\partial T_m/\partial y$, and (c) $-[V'\partial T''/\partial y - (V'\partial T''/\partial y)_m]$.

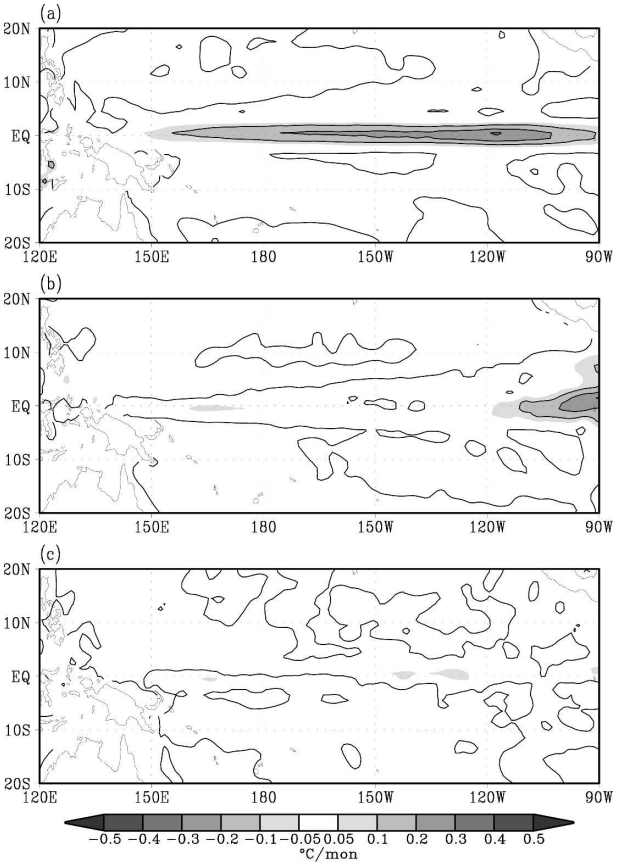

FIG. 10. Same as in Fig. 8, but for different components of the vertical heat advection: (a) $-W_m\partial T'_h/\partial z$, (b) $-W'\partial T_{\rm hm}/\partial z$, and (c) $-[W'\partial T'_h/\partial z\text{-}(W'\partial T'_h/\partial z)_m]$.

model simulations, we will further examine both temporal and spatial evolution of different advective terms in the heat budget in (3)–(5).

5. Mechanism of the slow evolution of the ENSO cycle

a. The thermocline and zonal advective feedbacks of the ENSO cycle

In section 4a, an analysis of temporal evolution of forcing terms, area-averaged over the Niño-3.4 region, was discussed. In section 4b, the spatial structure of horizontal and advective forcing was described. As also found in Jin and An (1999), the two dominating SST-tendency terms are the anomalous vertical advection by mean upwelling and the anomalous zonal advection by the mean zonal current. In this section, we further examine the spatiotemporal evolution of the dominant SST–tendency terms. This analysis keys on the lead–lag regression with the Niño-3.4 SST anomalies in the month of January (i.e., mature phase of a warm event) with some key terms in (3)–(5). The SST–tendency terms are first computed on a gridpoint-by-gridpoint basis, and for a lead and lag of 12 successive months, are regressed onto the January Niño-3.4 SSTs. These covarying anomalies, for selected components of the anomalous zonal and vertical advections, averaged between 1°S and 1°N, are shown in Fig. 11. The narrower meridional average is motivated by the fact of the narrow meridional extent of importance of vertical advection (Fig. 10). The month "0" on the y axis in Fig. 11 corresponds to a simultaneous correlation with the January Niño-3.4 SSTs. Furthermore, negative months are for January Niño-3.4 SST leading the forcing, while the positive months are for January Niño-3.4 lagging the forcing.

To compare our analysis with Jin and An (1999) more directly, we consider separately the two zonal advection terms: the advection of mean SST by anomalous zonal current (Fig. 11b), which is often referred to as the indicator for the so-called advective feedback in

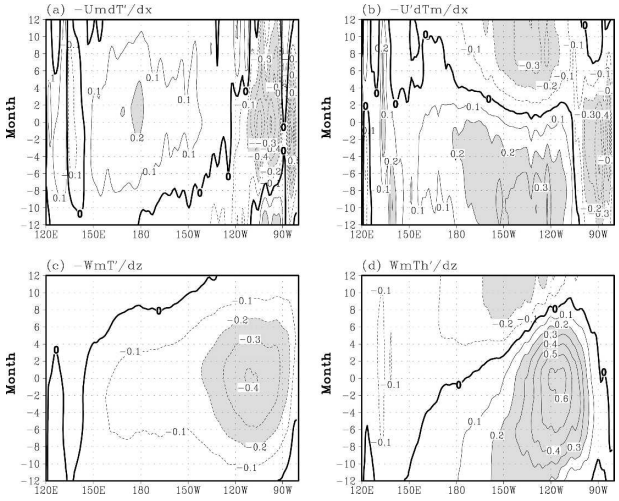

FIG. 11. Lead–lag regression for different forcing terms with the January Niño-3.4 SST index: (a) $-U_m\partial T'/\partial x$, (b) $-U'\partial T_m/\partial x$, (c) $-W_mT'/\Delta z$, and (d) $W_mT'_h/\Delta z$. The "0" month on the y axis indicates simultaneous regressions. Regressions are averaged between 1°S and 1°N. Shaded areas indicate where the regression is above the 95% significance level.

the tropical coupled ocean–atmosphere interaction (Jin and An 1999), and the advection of SST anomaly by mean current (Fig. 11a). We also analyze the anomalous vertical advection by the mean upwelling and further split this term into two: one related to damping of the SST anomalies by the mean upwelling (Fig. 11c), and the other term depicting the effect of mean upwelling to bring subsurface temperature anomalies to the surface (Fig. 11d). In a simple theoretical analysis based on Zebiak and Cane (1987, hereafter ZC)-type modeling framework, the second term is identified to be of critical importance for the ENSO cycle and is often referred as the indicator of the so-called thermocline feedback in the tropical coupled ocean–atmosphere interaction (cf. Jin and An 1999). This term also describes the most important dynamical feature in both delayed-oscillator and recharge oscillator paradigms.

Our analysis shows clearly that the mean upwelling is a damping term (Fig. 11c), but it is overcome by the thermocline feedback term (Fig. 11d). Moreover, in agreement with delayed-oscillator or recharge oscillator theory, the thermocline feedback term shown in Fig. 11d not only serves as the key positive feedback that overcomes the damping effect by mean upwelling, it is also one of the primary factors responsible for the ENSO phase turnaround. For instance, at 12 months prior to the peak warm phase of the ENSO, the term for the thermocline feedback already contributes to the initiation of warming, whereas 12 months after the peak warm phase, this term gives rise to a cooling tendency.

Analysis also indicates that the anomalous zonal advection plays an important role in the model-simulated ENSO cycle. Particularly, the evolution of the so-called zonal advective feedback term shown in Fig. 11b shows that this feedback is another important factor in ENSO phase turnaround, specifically in the equatorial central to eastern Pacific from 180° to 100°W. The significant contribution from this process was not envisioned in the earlier delayed-oscillator theory for ENSO but is consistent with the revised version of the Recharge Oscillator model (Jin and An 1999). The importance of this advective process is also partly consistent with the so-called advective–reflective oscillator (Picaut et al. 1997).

It should be noted that the advective feedback term tends to peak at about 12 months lead (lag), when the ENSO cycle is at its transition phase with little surface wind anomalies. Thus the anomalous zonal currents at this time are largely a result of the anomalous warm (cold) equatorial ocean heat content, as one can infer from the geostrophic balance. Following Jin and An (1999), we further examine in Fig. 12 the vertical averaged ocean currents above 300 m together with the sea surface height anomalies at peak and transition phases. A vertical average over the top 300 m was chosen because the vertically averaged currents are a close indicator of Sverdrup transport in response to the equatorial upper-ocean mass redistribution. Consistent with the finding in Jin and An (1999) from the ocean reanalysis data, there is an equatorial eastward (westward) ocean zonal current anomaly that accompanies the positive (negative) equatorial sea surface height anomalies at the 12 lead (lag). While at the peak warm phase, there is also clear indication of diverging meridional ocean current. Thus, the results shown in Figs. 11b,d, and in Fig. 12, are entirely consistent with those in Jin and An (1999). Our model results seem to support qualitatively the ENSO mechanism depicted in the revised recharge oscillator.

The role of zonal advection by mean zonal currents as shown in Fig. 11a appears to play a similar role as the meridional advection by mean meridional current in spreading the SST anomaly from the eastern Pacific toward the western Pacific. The impact of this process appears to be relatively minor in comparison with the other terms. Nevertheless, it may have an impact on the stability and periodicity of ENSO cycle through the coupled interactions, a prospect worth further theoretical studies.

To summarize, further examination of mixed-layer temperature tendency suggests that there are two key SST–tendency terms: the so-called thermocline feedback and the zonal advective feedback. These are the

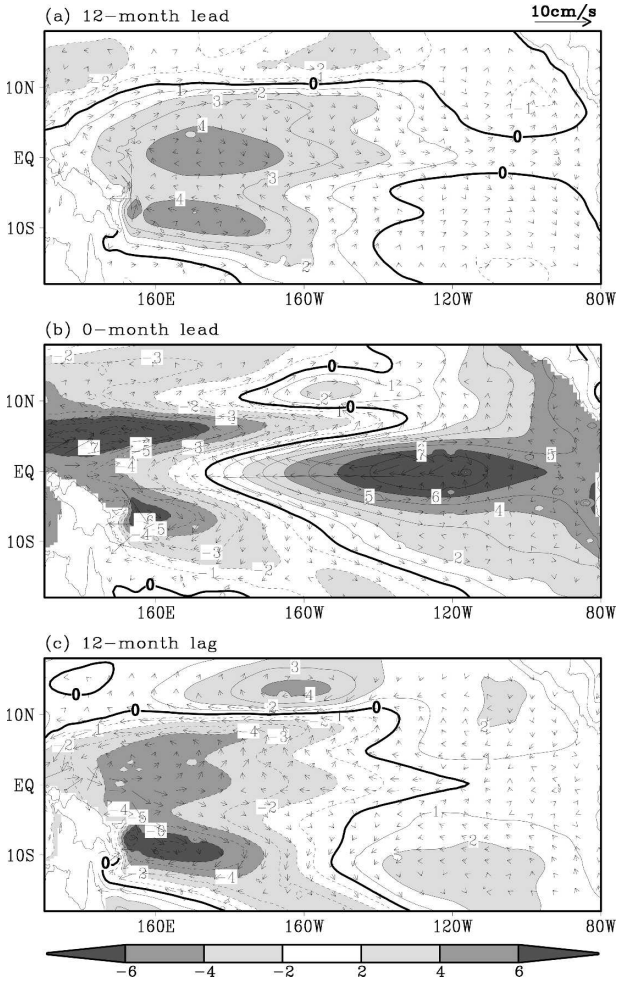

FIG. 12. Regression of the sea level height (shading) and ocean currents (averaged from surface to 300 m) with the Niño-3.4 SST index with (a) 12-month lead, (b) 0-month lead, and (c) 12-month lag for sea level height and current anomalies, separately (cm and cm s^{-1}). For the purpose of illustration, the meridional component of the ocean current is multiplied by 5.

main source for the positive feedback and are also the main factors responsible for the ENSO phase turnaround. Thus the main mechanism of the *slow ENSO cycle* simulated in the current version of the NCEP model is to a great extent consistent with the revised conceptual recharge oscillator proposed by Jin and An (1999), as illustrated schematically in Fig. 13.

The sequence of the model-simulated ENSO cycle can be described as follows: As aftermath of a cold event, shown in the bottom-left panel in Fig. 13, the surface temperature anomalies and associated equatorial wind anomalies have dissipated, but subsurface ocean temperature in the main thermocline is weakly warm along the entire equatorial region as the result of recharge of the ocean heat content during the cold phase. This recharge process is indicated by the arrows for meridional ocean currents in the bottom-right panel. The warm subsurface temperature anomalies in this transition phase are also accompanied by zonal ocean current anomalies, as can be inferred from the geostrophic balance. The anomalous vertical advection of the subsurface water by mean upwelling and anomalous zonal advection of mean SST by the anomalous eastward equatorial currents, as indicated in the bottom-left panel, provide the positive SST tendency to generate the positive SST anomalies and initiate the warm phase of the ENSO as shown in the upper-left panel in Fig. 13. When there are positive equatorial SST anomalies, the westerly wind anomalies follow. This allows an adiabatic redistribution of the subsurface ocean heat content such that thermocline depth in the warm pool region shoals and in the cold tongue region deepens, to give rise to cold and warm subsurface temperature anomalies in these regions, respectively. The SST anomalies are intensified by the anomalous vertical advection of even warmer subsurface temperature anomalies to the surface by mean upwelling. This development of the warm phase, however, is turned around as the result of discharge of the equatorial heat content during the warm phase. This discharge process is indicated by the arrows for meridional ocean current anomalies in the top-left panel. The continuing discharge of the equatorial heat content, resulting from the wind-forced redistribution of the subsurface ocean heat content, not only leads to the demise of the warm phase, but also leaves a cold equatorial subsurface temperature anomaly in the entire tropical Pacific, as indicated in the top-right panel. The cold equatorial subsurface temperature anomalies are accompanied by westward zonal (geostrophic) current anomalies. This transition phase allows a cold SST tendency as the result of the anomalous vertical advection of the cold subsurface temperature anomalies by the mean upwelling and the anomalous zonal advection of the mean SST by the westward current anomalies. Together these two anomalous advection processes lead to a cold phase of the ENSO cycle.

b. The role of high-order vertical modes and subtropical ocean Rossby waves in the ENSO cycle

The composite analysis of the ENSO cycle in section 3, and its evolution based on the analysis of mixed-layer heat budget in sections 4a–b, describes a well-defined ENSO cycle in model simulations. Indeed, the time series of the Niño-3.4 SSTs from the coupled simulations illustrate a very periodic ENSO cycle in the model with warm and cold ENSO peaks repeating almost every

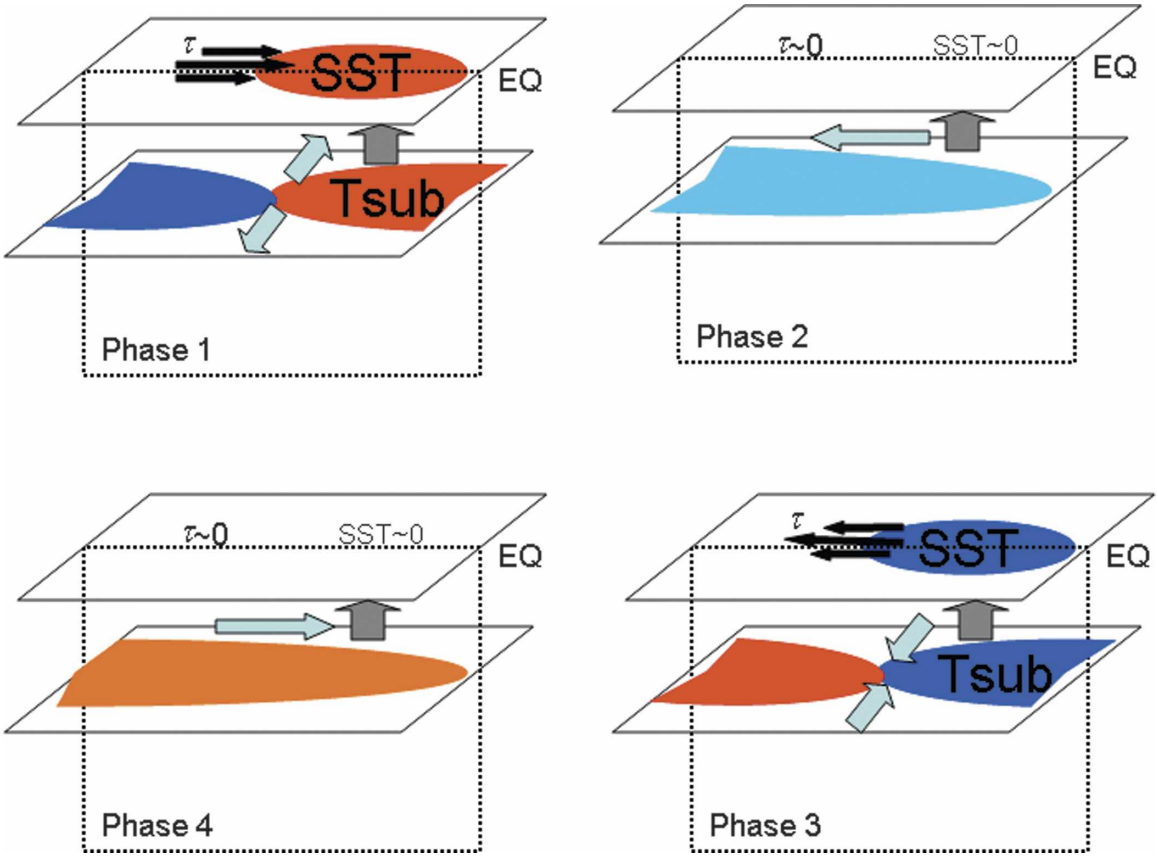

FIG. 13. Schematic diagram illustrating the recharge–discharge oscillator for the ENSO cycle. Phase 1 represents El Niño conditions and phase 3, the La Niña conditions. Phases 2 and 4 are transition conditions. The red and blue colors indicate the positive and negative SST and subsurface temperature anomalies, respectively. The black arrows represent the anomalous wind stress. The blue thick arrows represent the anomalous Sverdrup transport; the gray arrows indicate the climatological upwelling across the thermocline.

5 yr (see Fig. 7b dashed line). A hint for a periodic ENSO cycle is also evident in the vertical structure of the composited subsurface temperature anomalies and heat content anomalies in Figs. 3 and 4, where it can be seen that as the warm ENSO develops and propagates eastward, development of the ensuing cold phase of ENSO is already initiated in the western Pacific. Further examination of various SST tendency terms points to a relatively simple picture for the ENSO in our coupled model, a picture that is consistent with much simpler theoretical coupled models.

In this section, we further demonstrate that indeed the basic picture or basic mechanisms derived from a simple theoretical coupled model based on a ZC-type coupled framework appears to capture the essence of the ENSO cycle simulated in our much more complex coupled model. We take a very simple approach, namely, we will compare the correlation maps and covariance maps for the ocean heat content evolution associated with the model-simulated ENSO cycle. The panels in the right column of Fig. 14 are essentially equivalent to those in Fig. 3b. What is very striking in Fig. 14f (Fig. 14j), for instance, is the subsurface warm water (cold water) 12 month prior to (after) the peak warming at the surface at zero lag (middle panel). This feature is also evident in the left column for the correlations as well. There is however one significant difference comparing the panels of the left and right columns, that is, there is a clear signature of the second baroclinic mode structure in the correlation patterns in the left column, particularly from the central to the eastern equatorial Pacific. This is reflected in the opposite signs of the correlation in the top and bottom sections of the upper 300 m of the equatorial eastern Pacific, as seen most clearly in Figs. 14 d,e. However, this signal virtually disappears in the covariance plots in the right column, suggesting that this mode has only a minor contribution to the subsurface temperature anomalies that influence SSTs. Thus, we conclude that the high-order vertical mode of equatorial oceanic waves appears to play only a very minor role in the model-simulated ENSO cycle. This is perhaps a convincing model evi-

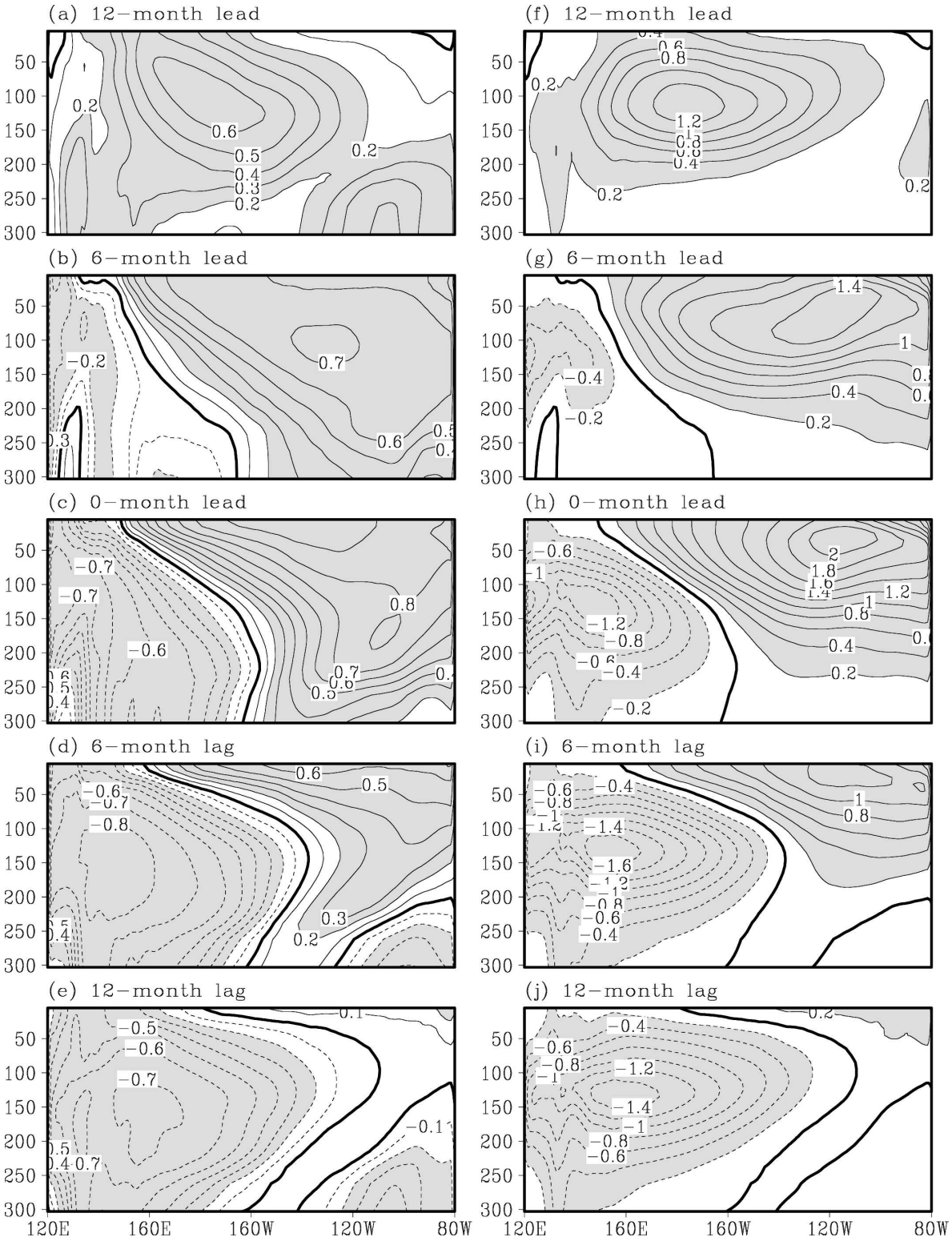

FIG. 14. (left) Correlation and (right) regression of the ocean temperature anomaly along the equator with the Niño-3.4 SST index in (a), (f) 12-month lead, (b), (g) 6-month lead, (c), (h) 0-month lead, (d), (i) 6-month lag, and (e), (j) 12-month lag. The shaded areas are the regions where the correlation coefficient is above the 95% significance level.

dence in support of the relevance of the simple ZC-type framework in which only the first baroclinic mode of equatorial wave dynamics is captured.

We extended a similar analysis by contrasting the correlation and covariance maps for the horizontal structures of upper-ocean heat content evolution. The main difference between the two, showed in Fig. 15, lies in the off-equatorial regions poleward of 15°S to 15°N. The correlation signal in the subtropical region, although weak, has a clear westward propagation and is a consequence of the subtropical ocean Rossby waves. From the contrast between the panels on the right and left in Fig. 15, it is clear that the subtropical Rossby waves, no matter whether they are forced by wind stress curl in the subtropical region, or are reflected at the eastern boundary from the equatorial Kelvin waves, contribute little to changes in the equatorial heat content, such as discharging and recharging of the equatorial heat content. Thus our simple analysis appears to be consistent with the finding from the analysis of the simple ZC-type model that ocean Rossby waves beyond 15°N and 15°S appear to be slaved to the ENSO cycle and do not actively contribute to the evolution of the ENSO cycle (e.g., Battisti 1988; Jin 1997b).

Although it is known from theoretical modeling that the higher-order vertical modes and subtropical ocean Rossby waves play little role in the ENSO cycle, we have demonstrated with a simple diagnostic method that this is also the case for the ENSO cycles simulated in the complex coupled model. Thus, the ENSO cycles simulated in our comprehensive coupled model share essentially the ENSO dynamics depicted in simple coupled models.

6. Summary and discussion

Based on a set of coupled model simulations, in this paper the evolution of model-simulated ENSO was analyzed. The analysis is of importance for at least the following two reasons: 1) coupled models are increasingly used to provide guidance for seasonal predictions, and for their optimal utilization, it is essential to understand the mechanisms (and biases) behind the model-simulated ENSO events; and 2) multiple theories for ENSO evolution have been proposed, and reliance on coupled models is an essential tool for understanding the relative importance of different ENSO mechanisms.

Our analysis was based on the evolution of composite ENSO events as well as on the analysis of the mixed-layer heat budget associated with ENSOs. The salient features of the model-simulated ENSO cycle were as follows:

- For the composite ENSO cycle simulated by the coupled model, the onset of warm ENSO events occurs approximately 6 months earlier than in the observations. This earlier onset is perhaps related to the fact that a model-simulated ENSO has a period of around 5 yr instead of about 4 yr in the observations.
- The heat budget of the mixed layer is primarily a sum of two large, but opposite terms: advections and the net surface heat flux.
- The net surface heat flux represents a damping term, that is, is opposite to the sign of the mixed-layer temperature anomaly. The largest term in the surface heat flux is the anomalous shortwave radiative heat flux.
- Among different advection terms, linear advection terms dominate. Zonal advection is dominated by the advection of climatological mixed-layer temperature due to the anomalous zonal currents. For the meridional advection, the most important contribution is by the advection of anomalous mixed-layer temperature by the climatological meridional ocean currents. This term is responsible for the meridional spread of equatorial SST anomalies. The anomalous vertical advection is narrowly confined to an equatorial strip and occurs because of the mean upwelling of the temperature anomaly below the mixed layer.
- The model simulations have a well-defined, and a very periodic, ENSO cycle. For example, almost all warm ENSO events are followed by cold ENSO events, and the cycle tends to repeat every 5 yr.
- The main positive feedback mechanism appears from the so-called thermocline feedback. Namely, warm (cold) equatorial SST anomalies gives rise to westerly (easterly) wind anomalies to the west of the SST anomaly; the latter produce warm (cold) subsurface ocean temperature anomalies by pressing down the isothermal surface (or thermocline depth) through adiabatic mass adjustment; and finally, these warm (cold) subsurface temperature anomalies are brought up to the surface by the mean upwelling to reinforce the SST anomalies.
- The ENSO phase transition largely results from two processes: the anomalous zonal advection of mean SST by anomalous zonal currents and anomalous vertical advection by mean upwelling, which brings the subsurface temperature anomalies to the surface. During the warm (cold) to cold (warm) ENSO phase transition, the equatorial subsurface oceanic temperature anomalies along the entire equator are already cold (warm) owing to the excessive discharge (recharge) during the warm (cold) phase. This cold (warm) equatorial subsurface temperature anomaly is also accompanied by anomalous eastward (west-

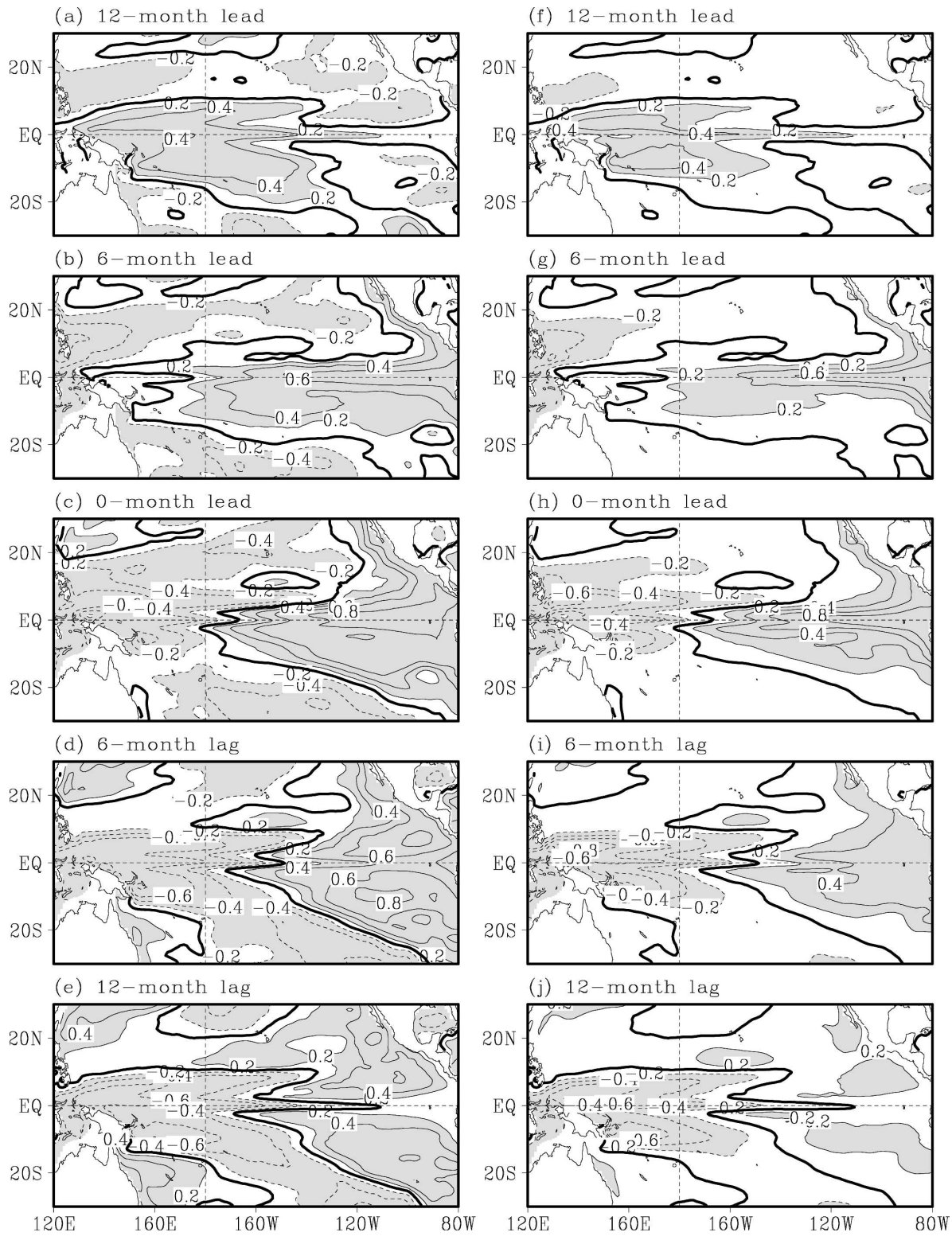

FIG. 15. Same as in Fig. 14, except for subsurface heat content anomaly.

ward) equatorial zonal current anomalies. Both the cold (warm) equatorial subsurface temperature and eastward (westward) zonal currents bring a warm to cold (cold to warm) ENSO phase transition. Thus model-simulated ENSO mechanisms are largely consistent with the revised recharge oscillator model of Jin and An (1999).

- Our analysis also lends further support that high-order vertical modes and subtropical ocean Rossby waves play little role in the ENSO cycles. Overall, the ENSO simulated in the complex model shares similar mechanisms identified in the much simpler coupled models.

The coupled model analyzed in this study has larger than observed high-frequency atmospheric noise (or variability), and associated phenomena, for example, westerly wind events. For instance the variance of intraseasonal variability is significantly larger than what is observed (not shown). This high-frequency variability simulated in the coupled model seems to have little consequence on the evolution of the model-simulated ENSO cycle (Wang et al. 2005) and is probably a result of the dominant role of coupled ocean–atmosphere interactions and their control on the model-simulated ENSO cycle.

There are still a number of issues that remain unclear. For instance, what controls the periodicity of the ENSO cycle? Why it is around 5 yr and why is it so regular even in the presence of a considerable amount of high-frequency noise? ENSO simulations by other CGCMs have also been analyzed in a number of studies (Latif et al. 2001; AchutaRao and Sperber 2001; Delecluse et al. 1998). Overall, in most CGCMs the simulated ENSOs are either too weak in amplitude or occur too frequently. In addition, many models fail to reproduce the observed seasonal phase locking of ENSO events that generally tends to peak near the end of the calendar year. In contrast, the NCEP CFS realistically captured the seasonal phase locking, but with stronger amplitude and a longer period. However, as for many other coupled CGCMs, the simulated interannual variability in the western Pacific (far eastern Pacific) in the NCEP CFS was too strong (weak). The reasons for the deficiencies of this coupled model remain unclear. Further analysis of the coupled model simulations together with some sensitivity of simulated ENSO to the climate mean state may provide further insight into some of these questions.

Acknowledgments. Support provided by the NOAA OGP's "Climate Dynamics and Experimental Prediction" program is gratefully acknowledged. FFJ is supported by NSF Grant ATM-0226141 and NOAA Grant GC01- 246.

REFERENCES

AchutaRao, K., and K. R. Sperber, 2001: Simulation of the El Niño Southern Oscillation: Results from the Coupled Model Intercomparison Project. *Climate Dyn.,* **19,** 191–209.

An, S.-I., and F.-F. Jin, 2001: Collective role of thermocline and zonal advective feedbacks in the ENSO mode. *J. Climate,* **14,** 3421–3432.

Battisti, D. S., 1988: The dynamics and thermodynamics of a warming event in a coupled tropical atmosphere–ocean model. *J. Atmos. Sci.,* **45,** 2889–2919.

——, and A. C. Hirst, 1989: Interannual variability in the tropical atmosphere ocean system: Influence of the basic state and ocean geometry. *J. Atmos. Sci.,* **46,** 1687–1712.

Bjerknes, J., 1969: Atmospheric teleconnections from the equatorial Pacific. *Mon. Wea. Rev.,* **97,** 163–172.

Bonjean, F., 2001: Influence of surface currents on the sea surface temperature in the tropical Pacific Ocean. *J. Phys. Oceanogr.,* **31,** 943–961.

——, and G. S. E. Lagerloef, 2002: Diagnostic model and analysis of the surface currents in the tropical Pacific Ocean. *J. Phys. Oceanogr.,* **32,** 2938–2954.

Delcroix, T., J.-P. Boulanger, F. Masia, and C. Menkes, 1994: Geosat-derived sea level and surface current anomalies in the equatorial Pacific during the 1986–1989 El Niño and La Niña. *J. Geophys. Res.,* **99,** 25 093–25107.

Delecluse, P., M. K. Davey, Y. Kitamura, S. G. H. Philander, M. Suarez, and L. Bengtsson, 1998: Coupled general circulation modeling of the tropical Pacific. *J. Geophys. Res.,* **103,** 14 357–14 373.

Frankignoul, C., F. Bonjean, and G. Reverdin, 1996: Interannual variability of surface currents in the tropical Pacific during 1987–1993. *J. Geophys. Res.,* **101,** 3629–3647.

Gent, P. R., and J. C. McWilliams, 1990: Isopycnal mixing in ocean circulation models. *J. Phys. Oceanogr.,* **20,** 150–155.

Griffies, S. M., A. Gnanadesikan, R. C. Pacanaowski, V. Larichev, J. K. Dukowicz, and R. D. Smith, 1998: Isoneutral diffusion in a *z*-coordinate ocean model. *J. Phys. Oceanogr.,* **28,** 805–830.

Hasegawa, T., and K. Hanawa, 2003: Heat content variability related to ENSO events in the Pacific. *J. Phys. Oceanogr.,* **33,** 407–421.

Hayes, S. P., L. J. Mangum, J. Picaut, A. Sumi, and K. Takeuchi, 1991: TOGA-TAO: A moored array for real-time measurements in the tropical Pacific Ocean. *Bull. Amer. Meteor. Soc.,* **72,** 339–347.

Hirst, A. C., 1988: Slow instabilities in tropical ocean basin–global atmosphere models. *J. Atmos. Sci.,* **45,** 830–852.

Jin, F.-F., 1996: Tropical ocean-atmosphere interaction, the Pacific cold tongue, and the El Niño Southern Oscillation. *Science,* **274,** 76–78.

——, 1997a: An equatorial ocean recharge paradigm for ENSO. Part I: Conceptual model. *J. Atmos. Sci.,* **54,** 811–829.

——, 1997b: An equatorial ocean recharge paradigm for ENSO. Part II: A stripped-down coupled model. *J. Atmos. Sci.,* **54,** 830–847.

——, and S.-I. An, 1999: Thermocline and zonal advective feedbacks within the equatorial ocean recharge oscillator model for ENSO. *Geophys. Res. Lett.,* **26,** 2989–2992.

Kanamitsu, M., W. Ebisuzaki, J. Woollen, S.-K. Yang, J. J. Slingo,

M. Fiorino, and G. L. Potter, 2002: NCEP–DOE AMIP-II Reanalysis (R-2). *Bull. Amer. Meteor. Soc.,* **83,** 1631–1643.

Kang, I.-S., and S.-I. An, 2001: A systematic approximation of the SST anomaly equation for ENSO. *J. Meteor. Soc. Japan,* **79,** 1–10.

Kessler, W. S., and M. J. McPhaden, 1995: Oceanic equatorial waves and the 1991–93 El Niño. *J. Climate,* **8,** 1057–1072.

Large, W. G., J. C. McWilliams, and S. C. Doney, 1994: Oceanic vertical mixing: A review and a model with nonlocal boundary layer parameterization. *Rev. Geophys.,* **32,** 363–403.

Latif, M., and Coauthors, 2001: ENSIP: The El Nino simulation intercomparison project. *Climate Dyn.,* **18,** 255–276.

Lau, N. C., S. G. H. Philander, and M. J. Nath, 1992: Simulation of ENSO-like phenomena with a law-resolution coupled GCM of the global ocean and atmosphere. *J. Climate,* **5,** 284–307.

Levitus, S., and T. P. Boyer, 1994: *Temperature.* Vol. 4, *World Ocean Atlas 1994,* NOAA Atlas NESDIS 4, 117 pp.

McPhaden, M. J., and J. Picaut, 1990: El Niño–Southern Oscillation displacements of the western equatorial Pacific warm pool. *Science,* **250,** 1385–1388.

Pacanowski, R. C., and S. M. Griffies, 1998: MOM 3.0 Manual. NOAA/Geophysical Fluid Dynamics Laboratory, 680 pp.

Philander, S. G. H., 1990: *El Niño, La Niña and the Southern Oscillation.* Academic Press, 293 pp.

Picaut, J., M. Ioualalen, C. Menkes, T. Delcroix, and M. J. McPhaden, 1996: Mechanism of the zonal displacements of the Pacific warm pool: Implications for ENSO. *Science,* **274,** 1486–1489.

——, F. Masia, and Y. duPenhoat, 1997: An advective–reflective conceptual model for the oscillatory nature of ENSO. *Science,* **277,** 663–666.

Rasmusson, E. M., and T. H. Carpenter, 1982: Variations in tropical sea surface temperature and surface wind fields associated with the Southern Oscillation–El Niño. *Mon. Wea. Rev.,* **110,** 354–384.

Saha, S., and Coauthors, 2006: The NCEP Climate Forecast System. *J. Climate,* **19,** 3483–3517.

Smagorinsky, J., 1963: General circulation experiments with the primitive equations: I. The basic experiment. *Mon. Wea. Rev.,* **91,** 99–164.

Solomon, A., and F.-F. Jin, 2005: A study of the impact of off-equatorial warm pool SST anomalies on ENSO cycles. *J. Climate,* **18,** 274–286.

Suarez, M. J., and P. S. Schopf, 1988: A delayed action oscillator for ENSO. *J. Atmos. Sci.,* **45,** 3283–3287.

Vialard, J., C. Menkes, J. P. Boulanger, P. Delecluse, E. Guilyardi, M. J. McPhaden, and G. Madec, 2001: A model study of oceanic mechanisms affecting equatorial Pacific sea surface temperature during the 1997–98 El Niño. *J. Phys. Oceanogr.,* **31,** 1649–1675.

Wang, B., and Q. Zhang, 2002: Pacific–East Asian teleconnection. Part II: How the Philippine Sea anomalous anticyclone is established during El Niño development. *J. Climate,* **15,** 3252–3265.

——, R. Wu, and R. Lukas, 2000: Annual adjustment of the thermocline in the tropical Pacific Ocean. *J. Climate,* **13,** 596–616.

Wang, C., and R. H. Weisberg, 1994: On the "slow mode" mechanism in ENSO-related coupled ocean–atmosphere models. *J. Climate,* **7,** 1657–1667.

——, and J. Picaut, 2004: Understanding ENSO physics—A review. *Earth's Climate: The Ocean-Atmosphere Interaction, Geophys. Monogr.,* Vol. 147, Amer. Geophys. Union, 21–48.

Wang, W., and M. J. McPhaden, 2000: The surface-layer heat balance in the equatorial Pacific Ocean. Part II: Interannual variability. *J. Phys. Oceanogr.,* **30,** 2989–3008.

——, S. Saha, H. L. Pan, S. Nadiga, and G. White, 2005: Simulation of ENSO in the new NCEP Coupled Forecast System Model (CFS03). *Mon. Wea. Rev.,* **133,** 1574–1593.

Weisberg, R. H., and C. Wang, 1997: Slow variability in the equatorial west-central Pacific in relation to ENSO. *J. Climate,* **10,** 1998–2017.

Wyrtki, K., 1975: El Niño—The dynamic response of the equatorial Pacific Ocean to atmospheric forcing. *J. Phys. Oceanogr.,* **5,** 91–103.

Yu, J. Y., and C. R. Mechoso, 2001: A coupled atmosphere–ocean GCM study of the ENSO cycle. *J. Climate,* **14,** 2329–2350.

Zebiak, S. E., and M. A. Cane, 1987: A model El Niño–Southern Oscillation. *Mon. Wea. Rev.,* **115,** 2262–2278.